Available online at www.sciencedirect.com
SCIENCE DIRECT®
International Journal of Heat and Mass Transfer 48 (2005) 4010–4018
International Journal of HEAT and MASS TRANSFER
www.elsevier.com/locate/ijhmt

Free convection in a liquid-encapsulated molten semiconductor in a vertical magnetic field

Mei Yang, Nancy Ma *

Department of Mechanical and Aerospace Engineering, North Carolina State University, Campus Box 7910, Raleigh, NC 27695, USA

Received 20 December 2004; received in revised form 1 April 2005

Abstract

This paper treats the free convection in a layer of boron oxide, called a liquid encapsulant, which lies above a layer of a molten compound semiconductor (melt) between cold and hot vertical walls in a rectangular container with a steady vertical magnetic field. The magnetic field provides an electromagnetic (EM) damping of the molten semiconductor which is an excellent electrical conductor but has no direct effect on the motion of the liquid encapsulant. The competition between the two free convections determines the direction of the velocity of the interface.

1. Introduction

Electronic and optical devices are fabricated on wafers sliced from single-crystal ingots of compound semiconductor crystals. Since the performance of any device depends critically on the uniformity of the local concentration in the wafer on which it is produced, a major objective during the solidification of any semiconductor crystal is to minimize segregation in the crystal. The segregation in the crystal depends on the diffusive and convective transport of species in the melt, which depends on the motion of the molten semiconductor (melt). Since molten semiconductors are excellent electrical conductors, the melt motion can be damped and controlled by a steady (DC) magnetic field in order to control the species distribution in the crystal.

During the magnetic liquid-encapsulated Czochralski (MLEC) growth of compound semiconductor crystals, such as indium–phosphide (InP), phosphorus gas is bubbled at high pressure through an indium melt, and the indium and phosphorus fuse to form the compound InP. A layer of boron oxide (B_2O_3) encapsulates the melt to prevent escape of the volatile component (P). A single-crystal seed is lowered through the encapsulant which initiates solidification and crystal growth begins in the presence of an externally applied vertical magnetic field. This is an extremely important process because it was the first to produce 8-cm diameter twin-free indium–phosphide crystals which was accomplished by using magnetic stabilization [1,2]. Morton et al. [3] presented a model of dopant transport during the MLEC process. Understanding transport mechanisms during this important process has motivated studies of simplified two-dimensional flows which capture the basic physics that may be analogous to flows in an azimuthal plane in a realistic cylindrical system. Previous researchers have investigated the effect of a steady magnetic field on free convection in rectangular enclosures [4–11].

* Corresponding author. Tel.: +1 919 515 5231; fax: +1 919 515 7968.
E-mail address: nancy_ma@ncsu.edu (N. Ma).

0017-9310/$ - see front matter © 2005 Elsevier Ltd. All rights reserved.
doi:10.1016/j.ijheatmasstransfer.2005.04.019

Nomenclature

B	magnetic flux density
c_p	specific heat in the melt
c_{pe}	specific heat in the liquid encapsulant
g	gravitational acceleration
Ha	Hartmann number in the melt
$\mathbf{j}$	dimensionless electric current density
j_z	dimensionless electric current density in the z direction
k	thermal conductivity of the melt
k_e	thermal conductivity of the liquid encapsulant
L	width of molten semiconductor or liquid encapsulant
N	interaction parameter in the melt
p	dimensionless pressure in the melt
p_e	dimensionless pressure in the liquid encapsulant
Pe_t	thermal Péclet number in the melt
Pe_{te}	thermal Péclet number in the liquid encapsulant
Re	Reynolds number in the liquid encapsulant
R_m	magnetic Reynolds number in the melt
T	dimensionless temperature in the melt
T_e	dimensionless temperature in the liquid encapsulant
T_c	temperature of the cold wall
T_h	temperature of the hot wall
U	characteristic velocity in the melt
U_e	characteristic velocity in the encapsulant
u	horizontal component of the dimensionless melt velocity
u_e	horizontal component of the dimensionless liquid-encapsulant velocity
v	vertical component of the dimensionless melt velocity
v_e	vertical component of the dimensionless liquid-encapsulant velocity
$\hat{\mathbf{v}}$	dimensionless velocity in the melt
$\hat{\mathbf{v}}_e$	dimensionless velocity in the liquid encapsulant
x	dimensionless horizontal coordinate
$\hat{\mathbf{x}}$	unit vector in the horizontal direction for the Cartesian coordinate system
Y	dimensionless vertical coordinate
$\hat{\mathbf{y}}$	unit vector in the vertical direction for the Cartesian coordinate system

Greek symbols

(ΔT)	difference between the hot wall's temperature and the cold wall's temperature
α	dimensionless depth of the melt
β	thermal volumetric expansion coefficient of the melt
β_e	thermal volumetric expansion coefficient of the liquid encapsulant
χ	rescaled dimensionless vertical coordinate in the liquid encapsulant
η	rescaled dimensionless vertical coordinate in the melt
ϕ	dimensionless electric potential in the melt
γ	dimensionless depth of the melt, plus the dimensionless depth of the liquid encapsulant
λ_β	ratio of the density times the thermal volumetric expansion coefficient in the liquid encapsulant to that in the melt
λ_k	thermal conductivity of the liquid encapsulant divided by the thermal conductivity of the melt
λ_μ	dynamic viscosity of the liquid encapsulant divided by the dynamic viscosity of the melt
ρ	density of the melt
ρ_e	density of the liquid encapsulant
μ	dynamic viscosity of the melt
μ_e	dynamic viscosity of the liquid encapsulant
μ_p	magnetic permeability of the melt
σ	electrical conductivity of the melt
ξ	rescaled dimensionless horizontal coordinate

In particular, Garandet et al. [9] and Alchaar et al. [10] treated two-dimensional free convection in a rectangular enclosure with a vertical magnetic field. Previous research which has treated systems that have liquid encapsulation have neglected any coupling between the free convections in the molten semiconductor and in the liquid encapsulant and assumed that the liquid encapsulant is stagnant [12,13]. Recently, Farrell and Ma [14] used an asymptotic analysis in order to investigate the interaction between the melt and the encapsulant in a rectangular enclosure with strong magnetic fields. Series and Hurle [15] and Walker [16] have reviewed the use of magnetic fields during semiconductor crystal growth.

Previously, we treated the simplified asymptotic equations which are valid for a strong magnetic field for which $Ha \gg 1$ [14]. Here, the Hartmann number is $Ha = BL(\sigma/\mu)^{1/2}$ where B is the magnetic flux density and L is the width of the molten semiconductor (melt) or liquid encapsulant while σ and μ are the melt's electrical conductivity and dynamic viscosity, respectively. We investigated the coupling between the free convection in the liquid encapsulant and the molten semiconductor in

a rectangular enclosure with a strong horizontal magnetic field. For a strong magnetic field, we were justified in neglecting effects of inertia and convective heat transfer [17]. In an asymptotic solution for the inertialess convectionless melt motion for $Ha \gg 1$, the melt is divided into (i) an inviscid core region, (ii) Hartmann layers with an $O(Ha^{-1})$ thickness carrying an $O(Ha^{-1})$ flow adjacent to the bottom wall and adjacent to the encapsulant–melt interface, and (iii) parallel layers with an $O(Ha^{-1/2})$ thickness carrying an $O(Ha^{1/2})$ flow adjacent to the hot and cold walls. The Hartmann layers have a simple, local, exponential structure, match any vertical core or parallel layer velocities, and satisfy the boundary conditions along the bottom wall and along the encapsulant–melt interface. We consistently neglected an $O(Ha^{-1})$ perturbation, neglected the Hartmann layers and relaxed the no-slip conditions along the core adjacent to the hot and cold walls.

In the present study, we investigate the free convection in the same configuration as Farrell and Ma [14]. This is a highly idealized model involving a two-dimensional flow. This investigation is very different from our previous asymptotic treatment because we use a numerical approach to treat the full equations in the entire volume of the melt so that our solution is valid for any value of the magnetic field strength. We no longer use any asymptotic approximation to treat any subregions of the flow. We present results for a range of magnetic field strengths and compare the results to the asymptotic solution of Farrell and Ma [14].

2. Problem formulation

This paper treats the two-dimensional free convection in two layers of fluid with a molten semiconductor (melt) encapsulated by a layer of boron oxide in a steady horizontal or transverse magnetic field $B\hat{\mathbf{y}}$. Here, B is the magnetic flux density while $\hat{\mathbf{x}}$ and $\hat{\mathbf{y}}$ are the unit vectors for the Cartesian coordinate system. Our dimensionless problem is sketched in Fig. 1. The coordinates and lengths are normalized by the length of the melt or boron oxide L, so that α and $(\gamma - \alpha)$ are the dimensionless depths of the melt and boron oxide, respectively. Along $x = 0$ and $x = 1$, the liquids are maintained at temperatures T_c and T_h, respectively, where $T_h > T_c$. The boundaries at $y = 0$ and $y = \gamma$ are thermal insulators. Here, the fluid flows are driven by the temperature difference so that the characteristic velocities for the free convection in the melt [18] and in the encapsulant are

$$U = \frac{\rho g \beta (\Delta T)}{\sigma B^2}, \tag{1a}$$

$$U_e = \frac{\rho_e g \beta_e (\Delta T) L^2}{\mu_e}, \tag{1b}$$

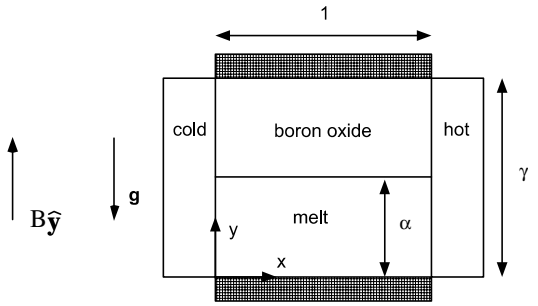

Fig. 1. Two-dimensional problem with a liquid encapsulant and molten semiconductor with a uniform, steady, vertical magnetic field $B\hat{\mathbf{y}}$ and with coordinates normalized by the distance between the hot and cold vertical walls.

respectively, where $(\Delta T) = T_h - T_c$ is the characteristic temperature difference and g is gravitational acceleration. Here, ρ, β and σ are the density, thermal volumetric expansion coefficient and electrical conductivity of the melt while ρ_e, β_e and μ_e are the density, thermal volumetric expansion coefficient and dynamic viscosity of the encapsulant. We use the thermophysical properties of molten indium–phosphide and boron oxide, as shown in Table 1. With $(\Delta T) = 50$ K and $L = 5$ cm [14], the characteristic velocity in the encapsulant is $U_e = 0.014065$ m/s while the characteristic velocity in the melt is 0.006282 or 0.00006284 m/s for $B = 0.5$ or 5 T, respectively.

The electric current in the melt produces an induced magnetic field which is superimposed upon the applied magnetic field produced by the external magnet. The characteristic ratio of the induced to applied magnetic field strengths is the magnetic Reynolds number, $R_m = \mu_p \sigma U L$, where μ_p is the magnetic permeability of the melt. For all crystal-growth processes, $R_m \ll 1$ and the additional magnetic fields produced by the electric currents in the melt are negligible.

Using the Boussinesq approximation, the free convection in the melt is governed by

$$N^{-1}(\mathbf{v} \cdot \nabla)\mathbf{v} = -\nabla p + T\hat{\mathbf{y}} + \mathbf{j} \times \hat{\mathbf{y}} + Ha^{-2}\nabla^2 \mathbf{v}, \tag{2a}$$

$$\nabla \cdot \mathbf{v} = 0, \tag{2b}$$

Table 1
Thermophysical properties of molten InP and B_2O_3

Property	Molten InP	B_2O_3
Viscosity (Pa s)	8.19×10^{-4}	10
Density (kg/m^3)	5050	1530
Specific heat (J/kg K)	424	1864.3
Thermal conductivity (W/m K)	22.8	2.0
Thermal volumetric expansion coefficient (K^{-1})	4.44×10^{-4}	7.5×10^{-5}
Electrical conductivity (Ω^{-1} m^{-1})	7×10^5	0.0

$$\nabla \cdot \mathbf{j} = 0, \tag{2c}$$

$$\mathbf{j} = -\nabla\phi + \mathbf{v} \times \hat{\mathbf{y}}, \tag{2d}$$

$$Pe_t(\mathbf{v} \cdot \nabla)T = \nabla^2 T, \tag{2e}$$

where $\mathbf{v} = u\hat{\mathbf{x}} + v\hat{\mathbf{y}}$ is the melt's velocity normalized by U, p is the deviation from hydrostatic pressure normalized by $\rho g\beta(\Delta T)L$, $\mathbf{j}$ is the electric current density normalized by σUB, ϕ is the electric potential normalized by UBL, and T is the deviation of the melt's temperature from T_c normalized by (ΔT). Eq. (2a) is the Navier–Stokes equation the interaction parameter $N = \sigma\beta^2 L/\rho U$ is the characteristic ratio of the electromagnetic (EM) body force term to the inertial terms. Eqs. (2b) and (2c) are conservation of mass and electric current, respectively. Eq. (2d) is Ohm's law for a vertical magnetic field. Eq. (2e) is the energy equation where the thermal Péclet number $Pe_t = \rho c_p UL/k$ is the characteristic ratio of convective to conductive heat transfer. Here, c_p and k are the melt's specific heat and thermal conductivity, respectively.

For the present plane recirculating flow in the melt, the condition of zero net electric current in the z direction in combination with electrically insulating boundaries implies that the electric field is zero [19]. The only non-zero component of the electric current density, normalized by σUB, is given by Ohm's law, $j_z = u$. For the present two-dimensional flow, this condition is very simple. In a real three-dimensional flow, electric currents in the z direction would close somewhere and generate a much more complex distribution of the electric potential ϕ.

With the Boussinesq approximation, the free convection in the encapsulant is governed by

$$Re(\mathbf{v}_e \cdot \nabla)\mathbf{v}_e = -\nabla p_e + T_e\hat{\mathbf{y}} + \nabla^2\mathbf{v}_e, \tag{3a}$$

$$\nabla \cdot \mathbf{v}_e = 0, \tag{3b}$$

$$Pe_{te}(\mathbf{v} \cdot \nabla)T_e = \nabla^2 T_e, \tag{3c}$$

where $\mathbf{v}_e = u_e\hat{\mathbf{x}} + v_e\hat{\mathbf{y}}$ is the encapsulant's velocity normalized by U_e, p_e is the deviation of the encapsulant's pressure from the hydrostatic pressure normalized by $\mu_e U_e/L$, and T_e is the deviation of the encapsulant's temperature from T_c normalized by (ΔT). Here, μ_e is the dynamic viscosity of the liquid encapsulant. Eq. (3a) is the Navier–Stokes equation where the Reynolds number $Re = \rho_e U_e L/\mu_e$ is the characteristic ratio of the inertial force to the viscous force in the encapsulant. Here, ρ_e is the encapsulant's density. Eq. (3b) is conservation of mass. Eq. (3c) is the energy equation where the encapsulant's thermal Péclet number $Pe_{te} = \rho_e c_{pe} U_e L/k_e$ is the characteristic ratio of convective to conductive heat transfer in the encapsulant. Here, c_{pe} and k_e are the specific heat and thermal conductivity of the encapsulant, respectively.

We apply the no-slip and no-penetration conditions along the walls at $x = 0$, $x = 1$, $y = 0$ and $y = \gamma$. Along the planar interface, the no-slip and no-penetration conditions [14] are

$$u(x,\alpha) = \frac{\lambda_\beta}{\lambda_\mu} Ha^2 u_e(x,\alpha), \quad \text{for } 0 \leqslant x \leqslant 1, \tag{4a}$$

$$v(x,\alpha) = 0, \quad \text{for } 0 \leqslant x \leqslant 1, \tag{4b}$$

$$v_e(x,\alpha) = 0, \quad \text{for } 0 \leqslant x \leqslant 1, \tag{4c}$$

where $\lambda_\beta = \rho_e\beta_e/(\rho\beta)$ and $\lambda_\mu = \mu_e/\mu$. With boron oxide and molten indium–phosphide, $\lambda_\beta = 0.051177$ and $\lambda_\mu = 12210$. The stress is continuous across the interface [14] so that

$$\frac{\partial u}{\partial y}(x,\alpha) = \lambda_\beta Ha^2 \frac{\partial u_e}{\partial y}(x,\alpha), \quad \text{for } 0 \leqslant x \leqslant 1. \tag{5}$$

Here, the gradients of the interfacial tension due to gradients of the temperature or of concentration along the encapsulant–melt interface are negligible [14].

The temperatures along $x = 0$ and $x = 1$ are the cold and hot wall temperatures, respectively, while the top and bottom of the container are insulated. The temperature and heat transfer in the melt and in the encapsulant are continuous across $y = \alpha$. Therefore, the thermal boundary conditions are

$$T(0,y) = 0, \quad \text{for } 0 \leqslant y \leqslant \alpha, \tag{6a}$$

$$T_e(0,y) = 0, \quad \text{for } \alpha \leqslant y \leqslant \gamma, \tag{6b}$$

$$T(1,y) = 1, \quad \text{for } 0 \leqslant y \leqslant \alpha, \tag{6c}$$

$$T_e(1,y) = 1, \quad \text{for } \alpha \leqslant y \leqslant \gamma, \tag{6d}$$

$$\frac{\partial T}{\partial y}(x,0) = 0, \quad \text{for } 0 \leqslant x \leqslant 1, \tag{6e}$$

$$\frac{\partial T_e}{\partial y}(x,\gamma) = 0, \quad \text{for } 0 \leqslant x \leqslant 1, \tag{6f}$$

$$T(x,\alpha) = T_e(x,\alpha), \quad \text{for } 0 \leqslant x \leqslant 1, \tag{6g}$$

$$\frac{\partial T_e}{\partial y}(x,\alpha) = \lambda_k \frac{\partial T_e}{\partial y}(x,\alpha), \quad \text{for } 0 \leqslant x \leqslant 1, \tag{6h}$$

where $\lambda_k = k_e/k$ where k and k_e are the thermal conductivities of the melt and the liquid encapsulant, respectively. With boron oxide and molten indium–phosphide, $\lambda_k = 0.08772$.

Eqs. (2)–(6) were solved using a Chebyshev spectral collocation method with Gauss–Lobatto collocation points in x and y. Since Eqs. (2a), (2e), (3a) and (3c) are non-linear, we used a Newton–Raphson iterative method. We used rescaled coordinates for our spectral

collocation method. Our rescaled horizontal coordinate is $\xi = 2x - 1$ so that $-1 \leqslant \xi \leqslant +1$. In the melt, our rescaled vertical coordinate is $\eta = (2y - \alpha)/\alpha$ so that $-1 \leqslant \eta \leqslant +1$. In the encapsulant, our rescaled vertical coordinate is $\chi = (2y - \gamma - \alpha)/(\gamma - \alpha)$ so that $-1 \leqslant \chi \leqslant +1$. We use a sufficient number of collocation points in order to resolve the velocity and temperature gradients. The number of collocation points in each direction in both the melt and the encapsulant were increased until the results were independent of these numbers. Of course, the required number of collocation points increased as B was increased because the thickness of the boundary layers decreased and the velocity gradients increased. The numbers of collocation points needed to resolve gradients in the parallel and Hartmann layers increase as B increases. The Gauss–Lobatto collocation points are coarse in the center of the domain at $\xi = 0$ and at $\eta = 0$ in the melt and at $\chi = 0$ in the encapsulant, and the collocation points become finer as $|\xi|$, $|\eta|$ or $|\chi|$ increase. For example, for $B = 0.5$ T and $\alpha = 0.3$, we used 41 collocation points in the horizontal direction, 41 collocation points in the vertical direction in the melt and 41 collocation points in the vertical direction in the encapsulant. When we increased the number of collocation points to 61 in each direction, the maximum value of the streamfunction in the melt changed by 0.000087%, the minimum value of the streamfunction in the encapsulant changed by 0.000021%, and the maximum value of the streamfunction in the encapsulant changed by 0.0015%.

3. Results

During the liquid-encapsulated Czochralski process, a molten semiconductor (melt) is contained in a crucible which is heated by radio-frequency induction heating. In order to keep the volatile component, i.e. P in InP, from escaping, the melt is encapsulated with liquid boron oxide. A single-crystal seed is lowered to the surface of the melt and initiates solidification. The crystal grows vertically downward into the melt and radially outward. Once the crystal reaches the desired diameter, the crystal is continuously "pulled" vertically upward until the entire melt's volume is solidified. Prior to solidification in the liquid-encapsulated Czochralski process, the axisymmetric melt is entirely encapsulated by the boron oxide. After a single-crystal seed initiates solidification and the crystal is pulled vertically upward, the encapsulant's depth increases and the melt's depth decreases due to solidification. Once the top of the crystal is pulled out of the encapsulant, the encapsulant's depth is constant while the melt's depth continues to decrease. The purpose of the present paper is to illustrate the degree of coupling for various magnetic field strengths so we only present results for $(\gamma - \alpha) = 0.2666$ and for a melt depth corresponding to the middle of growth for which $\alpha = 0.3$.

With the cold and hot walls along the left and right, respectively, the temperature gradient drives counterclockwise circulations in both the melt and the encapsulant. These circulations alone would lead to positive and negative values of u in the encapsulant and melt, respectively, adjacent to the interface. Therefore the shear stress σ_{xy} along the interface is always positive, i.e., a force to the left along the bottom of the encapsulant and an equal force to the right along the top of the melt. The competition between the two free convections, reflected by the continuity of u and of σ_{xy} along the interface, determines whether u along the interface is positive or negative. A positive value would reflect dominance by the melt circulation which results in a clockwise circulation in the encapsulant near the interface. For all cases considered here, the interfacial u is positive which reflects a dominance by the free convection in the encapsulant. This dominance increases as the magnetic field strength increases.

In Fig. 2, we present the dimensional interfacial shear stress for various magnetic flux densities. For $B = 0.5$ T, the free convection in the melt is relatively strong and produces a relatively large shear stress to the left along the bottom of the encapsulant. As the magnetic field strength is increased, the magnitude of the free convection in the melt decreases roughly as B^{-2}, as reflected by our choice for the characteristic velocity in Eq. (1a). This is reflected in the maximum magnitude of the melt velocity which is equal to 0.002733, 0.0009586, 0.0003461 and 8.045×10^{-5} m/s for $B = 0.5$, 1, 2 and 5 T, respectively, with $\alpha = 0.3$.

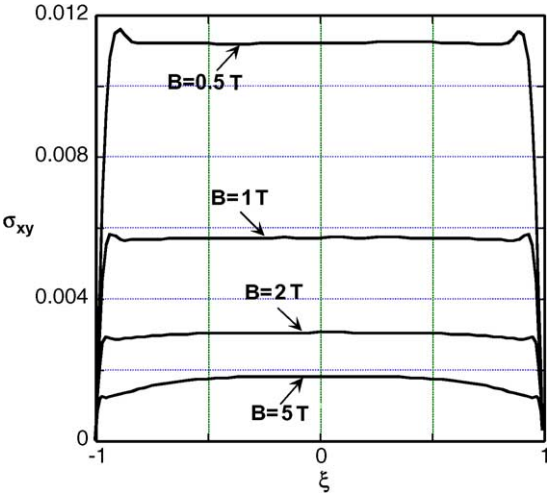

Fig. 2. Dimensional interfacial shear stress σ_{xy} (in Pa) versus ξ with $\alpha = 0.3$ for $B = 0.5$, 1, 2 and 5 T.

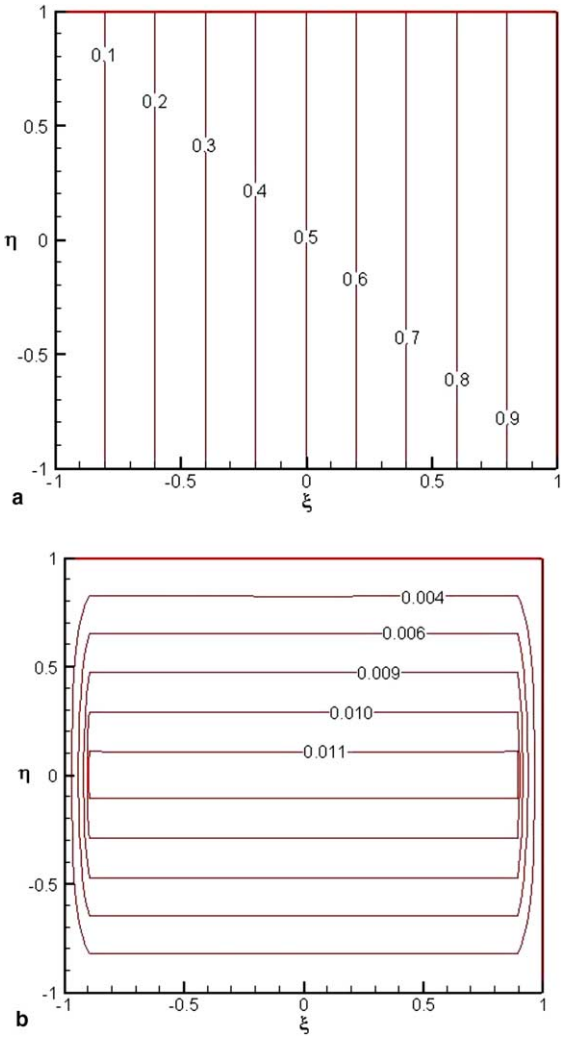

Fig. 3. Temperature and streamfunction in the melt for $B = 5$ T and $\alpha = 0.3$. (a) $T(\xi, \eta)$ and (b) $\psi(\xi, \eta)$.

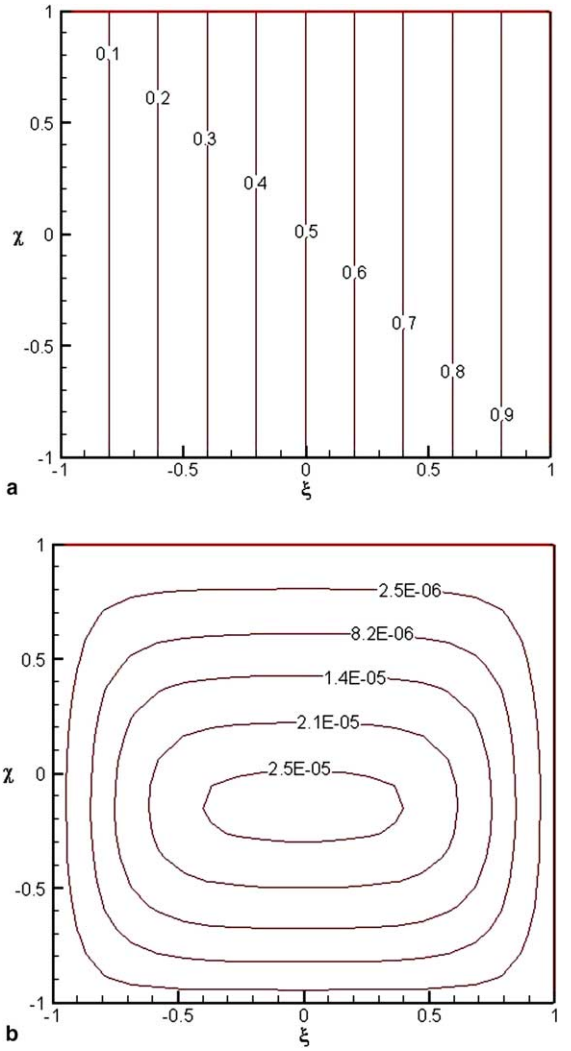

Fig. 4. Temperature and streamfunction in the encapsulant for $B = 5$ T and $\alpha = 0.3$. (a) $T_e(\xi, \chi)$ and (b) $\psi_e(\xi, \chi)$.

We present the contours of the temperature and the streamfunction in the melt for $B = 5$ T and $\alpha = 0.3$ in Fig. 3(a) and (b), respectively. The vertical isotherms in Fig. 3(a) reflect that the heat transfer is dominated by conduction in the melt. In Fig. 3(b), the maximum value of the streamfunction is 0.01120 and the circulation is counterclockwise, where the hot fluid rises adjacent to the hot wall along $\xi = +1$, flows to the left along $\eta = +1$, sinks adjacent to the cold wall along $\xi = -1$ and flows to the right along $\eta = -1$. We present the contours of the temperature and streamfunction in the encapsulant in Fig. 4(a) and (b), respectively. The vertical isotherms in Fig. 4(a) reflect that the heat transfer is dominated by conduction in the encapsulant. In Fig. 4(b), the maximum value of the streamfunction is 2.573×10^{-5} and the encapsulant flows in the counterclockwise direction. For this strong magnetic flux density, there is significant electromagnetic (EM) damping of the melt motion, and the maximum magnitude of the melt's velocity is 16 times larger than that of the encapsulant. The free convection in the encapsulant drives a positive interfacial velocity in the melt and a clockwise circulation inside the boundary layer along $\eta = +1$. $u = 0.07877$ along the interface at $\xi = 0$. The interfacial shear stress of the slow-moving melt decreases the velocity of the encapsulant but does not drive flow in the opposite direction.

When the magnetic flux density is decreased to $B = 1$ T, there is less EM damping of the melt motion and the velocity of the melt is larger. The maximum

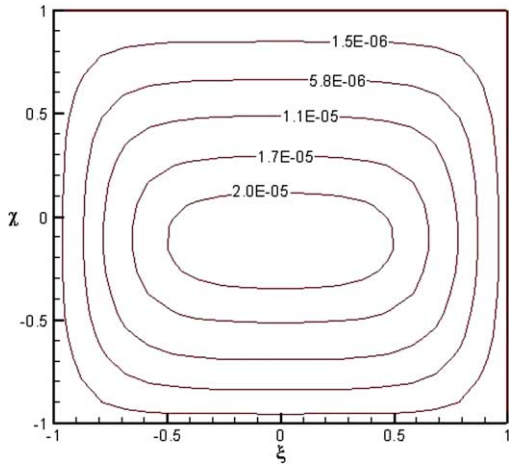

Fig. 5. Streamfunction in the encapsulant $\psi_e(\xi,\chi)$ for $B = 1$ T and $\alpha = 0.3$.

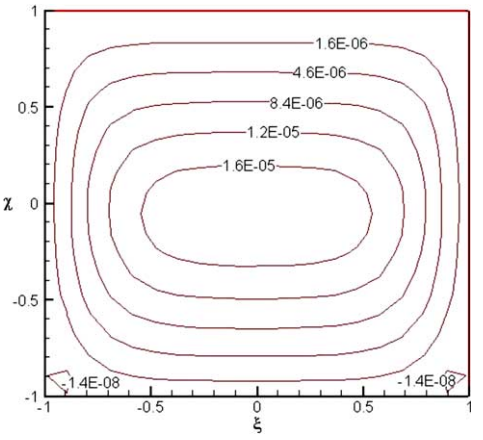

Fig. 6. Streamfunction in the encapsulant $\psi_e(\xi,\chi)$ for $B = 0.5$ T and $\alpha = 0.3$.

magnitude of the melt's velocity is 244 times larger than that of the encapsulant. The heat transfer is still dominated by conduction in both the melt and the encapsulant and the isotherms exactly resemble those in Figs. 3(a) and 4(a), respectively. The maximum values of the streamfunction in the melt and in the encapsulant are 0.01124 and 2.225×10^{-5}, respectively. The circulations in both the melt and the encapsulant are counterclockwise. We present the contours of the streamfunction in the encapsulant in Fig. 5. The free convection in the encapsulant drives a positive interfacial velocity in the melt and a clockwise circulation inside the boundary layer along $\eta = +1$, $u = 0.002321$ along the interface at $\xi = 0$. Although the melt moves more quickly in a 1 T field compared with a 5 T field, the interfacial shear stress more moderately decreases the velocity of the encapsulant but does not drive flow in the opposite direction.

When the magnetic flux density is decreased to $B = 0.5$ T, there is significantly less EM damping of the melt motion and the velocity of the melt is much larger. This is reflected in the maximum magnitude of the melt's velocity of 0.002733 m/s which is 966 times larger than the maximum magnitude of the encapsulant's velocity. The heat transfer is still dominated by conduction in both the melt and the encapsulant, and the circulation in the melt is counterclockwise. The maximum value of the streamfunction in the encapsulant is 1.759×10^{-5}. The circulation in the melt is still counterclockwise and the maximum value of the streamfunction in the melt is 0.01148. As shown in Fig. 2, the interfacial shear stress for $B = 0.5$ T is much larger than that for the other magnetic flux densities considered in this investigation. This large shear stress causes some reversal of the flow in the encapsulant adjacent to the interface at $\xi = \pm 1$, which is reflected in the contours of the streamfunction in the encapsulant presented in Fig. 6.

We compare our numerical solution of the full governing equations to our asymptotic solution [14] which is valid for $Ha \gg 1$. Therefore, our solution should approach that of Farrell and Ma [14] as we increase the magnetic flux density. In Figs. 7–9, we present the maximum value of the streamfunction in the melt, the minimum value of the streamfunction in the encapsulant, and the maximum value of the streamfunction in the encapsulant, respectively, versus magnetic flux density calculated by the present numerical solution and by the asymptotic solution.

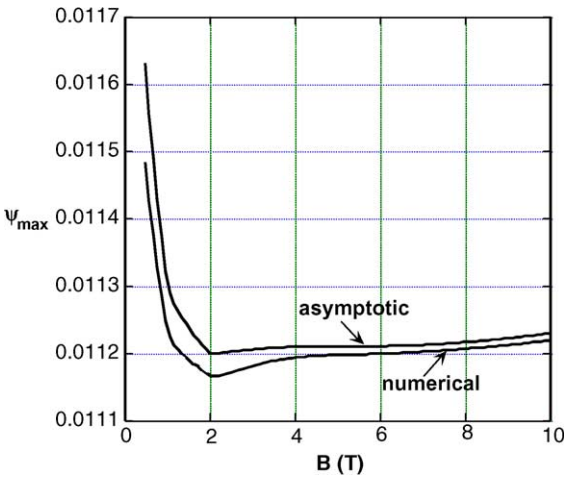

Fig. 7. Maximum value of the streamfunction in the melt versus magnetic field strength for the numerical and asymptotic solutions.

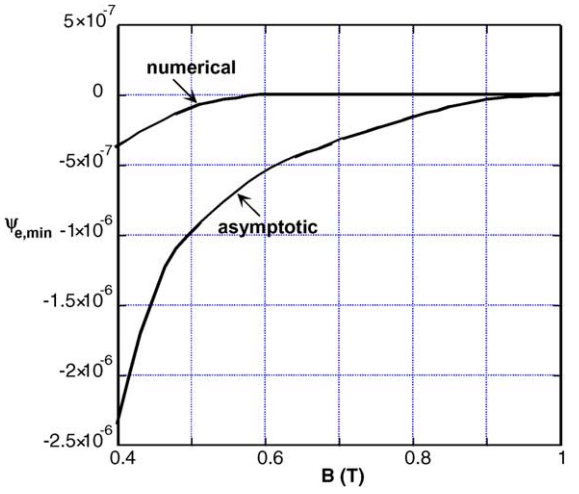

Fig. 8. Minimum value of the streamfunction in the encapsulant versus magnetic field strength for the numerical and asymptotic solutions.

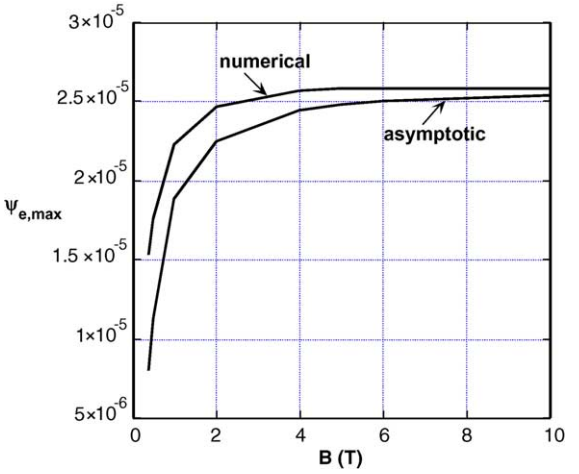

Fig. 9. Maximum value of the streamfunction in the encapsulant versus magnetic field strength for the numerical and asymptotic solutions.

4. Conclusions

The temperature gradient drives counterclockwise circulations in both the melt and encapsulant. These circulations alone would lead to positive and negative values of the horizontal velocity in the encapsulant and melt, respectively, near the interface. The competition between the two free convections determines the direction of the horizontal velocity of the interface. For $\alpha = 0.6$ and $B = 5$ T, there is significant EM damping of the melt motion and the encapsulant drives a positive interfacial velocity and a small clockwise circulation in the melt. For $\alpha = 0.6$ and a much weaker field $B = 0.5$ T, the maximum velocity in the melt is nearly one thousand times larger than that of the encapsulant, thus causing some of the encapsulant to circulate in the clockwise direction.

Acknowledgements

This research was supported by the US Air Force Office of Scientific Research under grant FA9550-04-1-0249. The calculations were performed on the Cray X1 and the SGI Origin 3000 Complex provided by the DoD High Performance Computing Modernization Program under grant AFSNH2487 and on the IBM pSeries 690 provided by the National Computational Science Alliance.

References

[1] D.F. Bliss, R.M. Hilton, J.A. Adamski, MLEK crystal growth of large diameter (100) indium phosphide, J. Cryst. Growth 128 (1993) 451–456.
[2] D.F. Bliss, R.M. Hilton, S. Bachowski, J.A. Adamski, MLEK crystal growth of (100) indium phosphide, J. Electron. Mater. 20 (1991) 967–971.
[3] J.L. Morton, N. Ma, D.F. Bliss, G.G. Bryant, Dopant segregation during liquid-encapsulated Czochralski crystal growth in a steady axial magnetic field, J. Cryst. Growth 242 (2002) 471–485.
[4] H. Ozoe, K. Okada, The effect of the direction of the external magnetic field on the three-dimensional natural convection in a cubical enclosure, Int. J. Heat Mass Transfer 32 (1989) 1939–1954.
[5] U. Burr, U. Müller, Rayleigh–Bénard convection in liquid metal layers under the influence of a vertical magnetic field, Phys. Fluids 13 (2001) 3247–3257.
[6] I. Di Piazza, M. Ciofalo, MHD free convection in a liquid-metal filled cubic enclosure. I. Differential heating, Int. J. Heat Mass Transfer 45 (2002) 1477–1492.
[7] G. Authie, T. Tagawa, R. Moreau, Buoyant flow in long vertical enclosures in the presence of a strong horizontal magnetic field. Part 2. Finite enclosures, Eur. J. Mech. B—Fluids 22 (2003) 203–220.
[8] R. Mossner, U. Muller, A numerical investigation of three-dimensional magnetoconvection in rectangular cavities, Int. J. Heat Mass Transfer 42 (1999) 1111–1121.
[9] J.P. Garandet, T. Alboussiére, R. Moreau, Buoyancy driven convection in a rectangular enclosure with a transverse magnetic field, Int. J. Heat Mass Transfer 35 (1992) 741–748.
[10] S. Alchaar, P. Vasseur, E. Bilgen, Natural convection heat transfer in a rectangular enclosure with a transverse magnetic field, J. Heat Transfer 117 (1995) 668–673.
[11] J.F. Kuniholm, N. Ma, Natural convection in a liquid-encapsulated molten semiconductor with a steady magnetic field, Int. J. Heat Fluid Flow 24 (2003) 130–136.

[12] N. Ma, J. Walker, D. Bliss, G. Bryant, Forced convection during liquid encapsulated crystal growth with an axial magnetic field, J. Fluids Eng. 120 (1998) 844–850.
[13] N. Ma, J.S. Walker, Liquid-metal buoyant convection in a vertical cylinder with a strong vertical magnetic field and with a nonaxisymmetric temperature, Phys. Fluids 7 (1995) 2061–2071.
[14] M.V. Farrell, N. Ma, Coupling of buoyant convections in boron oxide and a molten semiconductor in a vertical magnetic field, J. Heat Transfer 124 (2002) 643–649.
[15] R.W. Series, D.T.J. Hurle, The use of magnetic fields in semiconductor crystal growth, J. Cryst. Growth 113 (1991) 305–328.
[16] J.S. Walker, Models of melt motion, heat transfer and mass transport during crystal growth with strong magnetic fields, Prog. Cryst. Growth Charact. Mater. 38 (1999) 195–213.
[17] N. Ma, J.S. Walker, Inertia and thermal convection during crystal growth with a steady magnetic field, J. Thermophys. Heat Transfer 15 (2001) 50–54.
[18] L.N. Hjellming, J.S. Walker, Melt motion in a Czochralski crystal puller with an axial magnetic field: motion due to buoyancy and thermocapillarity, J. Fluid Mech. 182 (1987) 335–368.
[19] J.M. Hirtz, N. Ma, Dopant transport during semiconductor crystal growth. Axial versus transverse magnetic fields, J. Cryst. Growth 210 (2000) 554–572.